# The morphology of rigid polyurethane foam matrix and its evolution with time during foaming – New insight by cryogenic scanning electron microscopy

Joël Reignier, Pierre Alcouffe, Françoise Mechin, Françoise Fenouillot

# The Morphology of Rigid Polyurethane Foam Matrix and its Evolution with Time during Foaming– New Insight by Cryogenic Scanning Electron Microscopy

Joël Reignier[1,2], Pierre Alcouffe[1], Françoise Méchin[1], Françoise Fenouillot[1]

[1] *Univ Lyon, INSA-Lyon, CNRS, UMR 5223 IMP, F-69621, Villeurbanne, France*

[2] Author to whom correspondence should be addressed. E-mail: joel.reignier@polymtl.ca

**Abstract:** This paper presents an investigation of the morphology of growing polyurethane (PU) rigid foams during the very first seconds of the process by cryogenic scanning electron microscopy (cryo-SEM) performed at -150°C. The heterogeneous nature of the initial mixture has been revealed with the presence of sub-micron size physical blowing agent droplets (isopentane), µm size dispersed phase nodules, and large air bubbles dispersed in a continuous matrix. Following the evolution of the microstructure during foaming by cryo-SEM suggested that the isopentane liquid droplets (undissolved part of the physical blowing agent) did not vaporize to create their own bubbles. These observations were confirmed by showing that the number of air bubbles per unit volume (~$10^6$ bubble/$cm^3$) was similar to the cell population density of the final foam (~$10^6$ cell/$cm^3$), while the number of isopentane droplets initially present was found to be six orders of magnitude higher (~$10^{12}$ droplet/$cm^3$). This all means that isopentane molecules initially dissolved in the continuous phase diffuse into the pre-existing air bubbles with no energy barrier to overcome (non-classical nucleation) whereas the isopentane droplets simply act like reservoirs. Finally despite our best efforts, there is still some doubt whether polymeric 4,4'-diphenylmethane diisocyanate (PMDI) is dispersed in the polyol phase, or polyol dispersed in PMDI.

**Key words:** polyurethane, foam, cryogenic scanning electron microscopy (cryo-SEM), nucleation, emulsion, microstructure

Published in *Journal of Colloid and Interface Science* vol. **552**, 153-165 (2019).

## 1. Introduction

For over 50 years, rigid polyurethane foams have been extensively used for thermal insulation of domestic appliances and buildings. They are relatively easy to produce at an industrial scale and their insulation capabilities will keep polyurethane foam demand high in the future. In response to the Montreal Protocol (1989), the foam industry has moved steadily from low conductivity physical foaming agents such as chlorofluorocarbons (CFCs) and hydrochlorofluorocarbon (HCFCs), to less efficient but more environment-friendly components such as $CO_2$ (generated via the isocyanate-water reaction) and aliphatic hydrocarbons (pentane). As a consequence, much work has been done in an effort to understand the foaming process in order to improve the efficiency of PU foams and preserve their benefits. This was generally accomplished by studying the effects of the processing parameters and formulations on the ultimate thermal and mechanical properties of the final product. Foam morphology that is, more or less open structure, cells size, walls and struts thickness, are known to play a dominant role on the thermal characteristics. As a consequence, it is of particular importance to characterize as precisely as possible the morphology as well as to understand how cells are formed.

Microscopic techniques are helpful and widely used to attempt reaching these objectives. A conventional imaging technique such as scanning electron microscopy (SEM) is one of the most commonly used tools to characterize the cellular structure of PU rigid foams. Recently, a few authors used X-ray microtomography (μCT) combined with 3D image analysis to compare the cell characteristics (cell size distribution, shape anisotropy ratio, distribution of polymer between struts and cell walls) of PU rigid foams [1] or to generate a realistic model for micromechanical modelling of closed-cell polymeric foams[2]. Unfortunately, all these imaging techniques are limited to the examination of fully cured foam products.

A few attempts have recently been proposed to follow the evolution of microstructure during foaming. Minogue observed *in-situ* the effect of various parameters (blowing agent type and concentration, surfactant type and amount, catalyst level…) on the nucleation process of PU foams and its evolution with time by means of a PC-controlled camera attached to a stereo optical microscope [3]. The author made the distinction between nuclei (size range < 40 μm), spherical bubbles (size range between 40 and 150 μm) which undergo radial growth until they get close to each other and eventually cells with polyhedral shape (usually size range > 150 μm). However, the whole analysis seems ambiguous regarding the origin of nuclei: are they air bubbles entrapped during the mixing stage, or bubbles made of blowing agents molecules coming from dissolved gas? Clarification is needed. Whatever the case, it was demonstrated that the initial nuclei of the unreacted polyol mixture were independent of the surfactant type, that the concentration of $H_2O$ (chemical blowing agent) did not affect the amount and

the size of the bubbles and that increasing the concentration of cyclopentane (physical blowing agent) from 0 to 10 wt% increased the average bubble size from 27 to about 39 µm. Pardo-Alonso et al. used a non-standard technique, namely high-resolution microfocus X-ray radioscopy, to investigate the cellular structure evolution occurring during the reactive processing of rigid PU foams [4]. They put a small droplet of the mixed isocyanate-component and polyol-component into a very thin mold (0.6 mm thick) to limit the number of cells in the depth direction (2–3 maximum). Image analysis allowed these authors to monitor *in-situ* the evolution of cell size and cell population density (number of cells per unit of volume of the solid material) during foaming. Despite their interesting findings that showed that nucleation at initial foaming stages strongly dominates over the coalescence mechanism (not observed), the resolution of this X-ray apparatus does not seem to permit the observation of cell size below a dozen of micrometers.

Apparently, cryogenic scanning electron microscopy (cryo-SEM) has never been applied to explore the microstructure of nascent rigid PU foams and its evolution with time. However, cryo-SEM has become nowadays more and more accessible in many laboratories and seems to be the method of choice to study the morphology of a wide range of specimens (complex liquid, semi-liquid with or without pores) which are very sensitive and/or hydrated. For instance, Zhao et al. used cryo-SEM to examine the morphology and to qualitatively estimate the bubble density of drug-loaded foams (used to improve drug delivery efficiency to the skin) based on hydrofluoroalkanes (HFA 134a and HFA 227) emulsions stabilized with Pluronic surfactants [5]. Ivan'kova et al. used cryo-SEM to follow the formation of porous structure in chitosan sponges during the lyophilization process and demonstrated that the diameter of the pores and their wall thickness were controlled by pre-freezing temperature [6]. Caldwell et al. used cryo-SEM to examine in details the four-phase structure of ice cream: ice crystals, air cells, fat in an emulsified form, and a continuous serum phase were identified [7].

From a practical point of view, cryo-preparation for SEM is a relatively straightforward and rapid technique, involving no chemical processing or contact with solvents. However, it was pointed out in a few examples that artifacts, i.e. structures in the sample that are not present naturally but only occur during freezing of the specimen, may appear. Zbik et al. observed distinctive gaps between the surface of fine clay mineral particles in suspension in water and wondered whether these voids (50-100 nm thick) adjacent to the solid surfaces were the result of shrinkage (during freezing) or were gaseous coatings attached onto the surface of the solid clay mineral [8]. Estimation of the shrinkage within the temperature interval used (0.1% for $\Delta T$=-200K) shows possible reduction in size around 0.002-0.01 µm but the thickness of the void layer between solid particle and matrix was much larger, which makes unlikely that the gaseous layers adjacent to the solid surfaces are the result of shrinkage. This

assumption was lately confirmed by their removal through ultrasonic treatment. Mikula et al. used cryo-SEM to characterize emulsions and suspensions in the petroleum industry and warned against the overinterpretation of the morphology observed after freezing [9]. They gave examples where the seemingly-lamellar morphologies of particulate suspensions (made from fumed silica, alumina or quartz which are essentially spherical) were similar to that observed in clay suspensions while these other mineral systems had no propensity for edge-to-edge orientation. According to the authors, those particular alignments of particles found their origin in the freezing and/or the sublimation steps preceding cryo-SEM observations. The few examples just mentioned demonstrate that care must always be taken in the interpretation of the cryo-SEM images. Talmon concluded in his paper dedicated to the study of nanostructured liquids (microemulsions, liquid crystalline phases…) by cryogenic scanning electron microscopy that the possibility of artifacts formation is ever present and that artifacts may be formed not only during the sample preparation and transfer into the microscope, but also during imaging, as a result of electron-beam damage [10].

In spite of all the efforts towards the better understanding of rigid PU foaming process, the microstructure of the original emulsion and the formation of the porous structure are not sufficiently studied and described in the literature, in particular at very small-scale. Therefore, the aim of the present work was to investigate the morphology of the original liquid mixture and to follow its evolution during foaming by using the cryo-chamber in a scanning electron microscope. To the best of our knowledge, such *in-situ* experimental investigation has never been described in the literature and may provide valuable information.

## 2. Materials and methods

### *2.1. Materials*

The materials used in this study were obtained from commercial sources and were used as received from the supplier, without any further purification. A polyether polyol (Baymer VP.PU 29HB30, provided by Bayer) having a hydroxyl value (mg KOH/g of sample) of 585 and an average functionality $f \sim 3.3$ was used. The physical blowing agent, 2-methylbutane (Isopentane, boiling point 27.8°C, density 616 kg/m$^3$) with molar mass of 72.15 g/mol was kindly supplied by Inventec. Tap water was used as the chemical blowing agent. N,N-dimethylcyclohexylamine (DMCHA), a gelling and blowing catalyst, was supplied by Evonik. Tegostab B 84501, a polysiloxane-ether copolymer used as a surfactant was supplied by Evonik. Tris(1-chloro-2-propyl) phosphate (TCPP) from Shekoy was used as a flame retardant and for decreasing viscosity. The polymeric 4,4'-diphenylmethane diisocyanate (PMDI) Desmodur 44V70L (NCO content 31.2 wt%, isocyanate equivalent weight $M_{NCO}$ = 134.7 g/mol,

functionality 2.8 < f < 3.6) was provided by Bayer. The amount of PMDI required for the reaction with polyether polyol and water was calculated in order to obtain an initial NCO/OH ratio of 1.15.

*2.2. Preparation of samples and basic freezing methods*

First a premix (Part A) was prepared from polyol and all the different additives, excepted PMDI. After the addition of each additive (fire retardant, surfactant, chemical blowing agent, catalyst and physical blowing agent), the mixture was stirred for 5 seconds by means of an IKA rotating mixer fitted with a LENART disc (VOLLRATH GmbH - $\phi$ = 60 mm) at a speed of 2500 RPM. Foams were prepared by adding PDMI to the premix at the second stage. The exact amount of isocyanate (Part B) is added to the premix via a syringe (weighed before and after) and mixed at 4500 RPM for 5 s. The precise moment when the isocyanate is added is considered as the starting time. The various formulations are given in Table 1. Small quantities of the mixture are then poured directly into the SEM specimen holders and quickly frozen by plunging them into liquid nitrogen ($LN_2$), when the corresponding time *t* was recorded.

**Table 1**. Compositions of premix A and AB systems used in the preparation of PUR foams. The horizontal dashed line divides the premix A from the B-component. AB3 is different from AB1, isopentane is premixed with PMDI instead of polyol.

| | Sample | | | | |
|---|---|---|---|---|---|
| Components (wt parts) | A1 | A2 | AB1 | AB2 | AB3 |
| Polyether polyol 29HB30 | 90 | 90 | 90 | 90 | 90 |
| TCPP (flame retardant) | 10 | 10 | 10 | 10 | 10 |
| Silicone surfactant B84501 | 2.5 | 2.5 | 2.5 | 2.5 | 2.5 |
| Water | 1.4 | 1.4 | 1.4 | 1.4 | 1.4 |
| Catalyst DMCHA | 0.9 | 0.9 | 0.9 | 0.9 | 0.9 |
| Isopentane | 0 | 14.8 | 14.8 | 0 | 14.8 |
| PMDI based isocyanate | 0 | 0 | 170.74 | 170.74 | 170.74 |

*2.3. Kinetics of foam formation*

The reactivity of foam formation is traditionally followed by the physical change of the properties such as "cream time" ($t_{cream}$), "string time" ($t_{string}$) and "tack-free time" ($t_{tack\text{-}free}$). The cream time corresponds to the start of bubble rise. The string time is an estimation of gel time and corresponds roughly to the starting point of stable network formation. It can be practically estimated by the time when long strings of tacky material can be pulled away with a stick from the surface of the foam. At the tack-free time, the outer surface of the foam loses its stickiness. By definition, in the present work the foaming time corresponds to the interval of time between the start of mixing of parts A and B and the time when the sample was frozen in $LN_2$. The characteristic times of the various AB systems are reported in Table 2. In a general manner, the experimental error on the characteristic times is about $\pm$ 2, 3 and 5 s for the cream, string and tack-free times, respectively.

**Table 2.** Characteristic times of the various polyurethane foams

| AB system | cream time (s) | string time (s) | tack-free time (s) |
|---|---|---|---|
| AB1 | 20 | 80 | 130 |
| AB2 | 20 | 80 | 130 |
| AB3 | 30 | 120 | 130 |

*2.4. Microscopy of frozen samples*

While still under $LN_2$, the sample holder was quickly transferred to the cold-stage of the SEM cryo-preparation chamber (model Alto 2500 from Gatan, Inc.), where fracturing was performed using a precision rotary knife to create a fresh internal surface free of frost. The sample was then sputter-coated with about 10 nm platinum and transferred into the SEM chamber where it remained frozen during imaging on another cold-stage. The temperature of the cold-stage inside the electron microscope was maintained at -150°C. The scanning electron microscope (FEI, model Quanta 250) was operated at an accelerating voltage of 5kV and a low electron beam current to minimize electron beam damage during imaging. The working distance was around 10 mm and the images were exclusively obtained by using the secondary electron detector situated in the specimen chamber. Radiation artifacts were avoided by focusing on an area and transferring to an adjacent area for recording.

*2.5. Image Analysis*

A semi-automatic method of image analysis using ImageJ software (U.S. National Institutes of Health) was used to measure the diameter and/or the volume fraction of the dispersed phases. The size of the dispersed phases was defined as the diameter of a circle of area equivalent to the projected area of the dispersed phase. Since all dispersed phases and/or cells are not sectioned at their widest point, many appear smaller than they actually are. As a result, any experimental measurement of size obtained from those 2D images will therefore be skewed to smaller sizes. To take into account this statistical phenomenon, the average diameter was multiplied by a correction factor of x1.2739 (ASTM D 3576-98). On the other hand, the volume fraction of the dispersed phases was directly measured by the area fraction on the image without any correction, according to the most fundamental rule in stereology [11].

**3. Results**

*3.1. Morphology of premix A prepared with and without physical blowing agent*

A preliminary study was carried out without PMDI to facilitate the identification of the different phases.

*3.1.1. Premix A1 (without isocyanate nor physical blowing agent)*

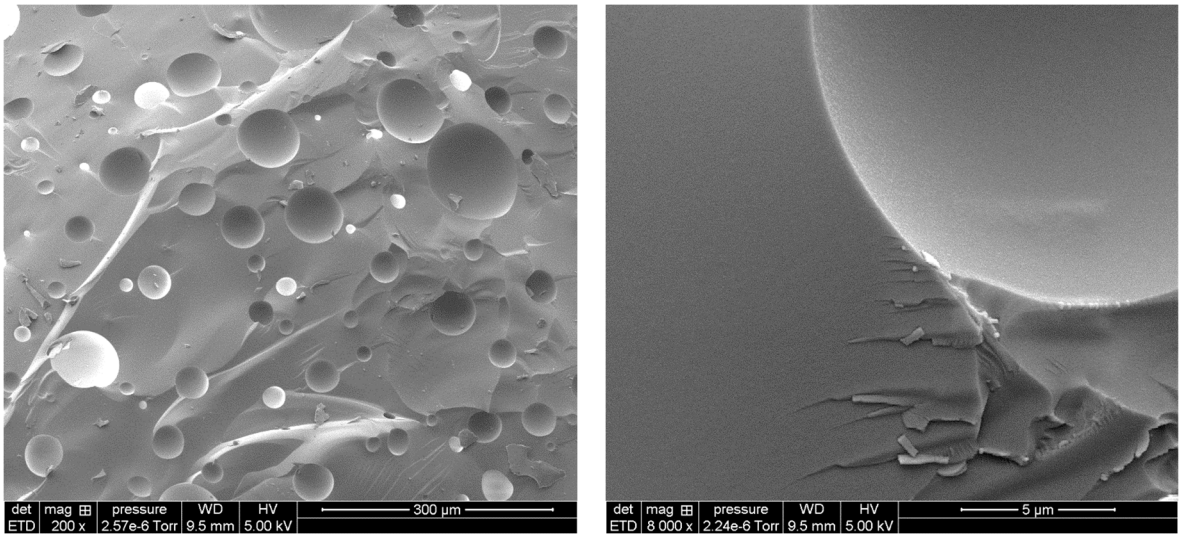


(a) (b)

**Fig. 1.** Cryo-SEM images of premix A1 (polyol + additives without isocyanate nor isopentane) showing the air bubbles at different magnifications (a) x200 and (b) x8000. The scale bars represent 300 and 5 µm, respectively.

Figure 1 shows typical cryo-SEM images of the morphology of premix A1 prepared with water but without isopentane. From this Figure, it can be seen that the large cavities corresponding to air bubbles entrapped into the system during mechanical agitation appear smooth and rounded, as expected for a liquid-gas surface directed by surface tension. Image analysis reveals that the average size of air bubbles is about 32 µm with bubble size varying between 5 and 125 µm (bubble size distribution is reported in Figure 3). For comparison purpose, quite similar bubble sizes (10 µm < $d$ < 100 µm) were obtained by Kanner for a one-shot flexible polyether formulation [12]. As expected, none of the additives (surfactant and flame-retardant chemicals) are visible inside the polyol matrix. They seem to be fully miscible inside the polyol within the concentration level investigated. The solubility limit was experimentally found to be greater than 100 wt% for TCPP in polyol.

*3.1.2. Premix A2 (with isopentane as blowing agent)*

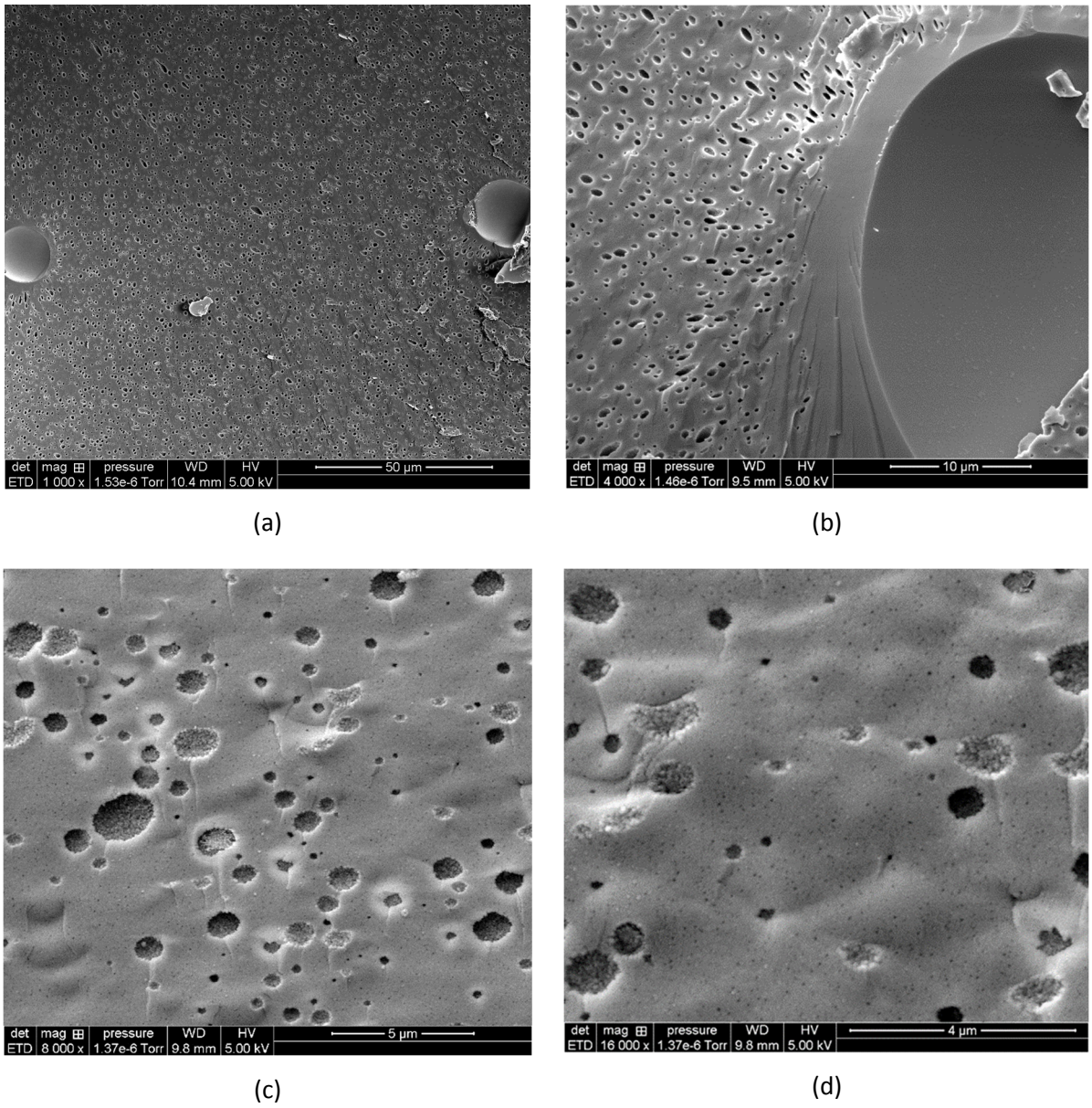


**Fig. 2.** Cryo-SEM micrographs of premix A2 (polyol + additives + isopentane) at different magnifications (a) x1000, (b) x4000, (c) x8000, (d) x16,000.

Consider now the morphology of the premix A2 with isopentane as physical blowing agent, as depicted in Figure 2. Large spherical shape cavities with a smooth internal surface can be seen in Figure 2a and Figure 2b and correspond to air bubbles, similar to those observed in Figure 1. More importantly, the polyol matrix is covered with a great number of small cavities with about 1 µm diameter. These micro-cavities are the reminiscence of the isopentane droplets and because of the large difference in size, they are easily distinguished from air bubbles. This result unambiguously indicates that a fraction of isopentane is not dissolved into the polyol phase. It is confirmed by our experimental estimation of the

solubility limit of isopentane in the polyol that was found to be around 8 wt% at room temperature (whereas the concentration of isopentane in premix A2 is about 12.4 wt%, see Table 1). Taking into account that the cryo-SEM experiments are conducted at temperature around -150°C and under high-vacuum conditions (P~$10^{-4}$ Pa), frozen pentane sublimates and leaves cavities in the solid polyol phase. Furthermore, it is worth mentioning that part of the isopentane molecules dissolved in the matrix may have diffused into air bubbles, according to Raoult's law. The higher magnification view (x8000) reported in Figure 2c provides finer imaging detail of the surface of isopentane cavities left by the sublimated isopentane droplets. The surface is not smooth as it was the case with air bubbles but the surface of the cavities appears rough, just as if it was covered with submicron spheres. Even if the origin of this roughness is unknown, it may be linked to the presence of surfactant molecules specifically located at the interface and which could remain partly embedded inside the polyol matrix after sublimation of isopentane. This phenomenon should be helpful to distinguish between isopentane droplets (liquid) and bubbles (gas). A careful observation of Figure 2d (x16000) reveals the presence of very small domains of nanometric size (≤ 100 nm) inside the polyol matrix, but it is hard to say if they are pores or not. Their absence in the premix A1 (without isopentane) suggests that they may correspond to isopentane clusters, possibly created by additional phase separation that occurred during freezing. The specific analysis of more than 500 of these nanodomains reveals an average diameter of about 29 nm with minimum and maximum values of 14 and 71 nm, respectively. For comparison purpose, the molecular diameter of an isopentane molecule is about 0.54 nm.

More quantitative results are reported in Figure 3 with the size distributions of isopentane (sublimated) pores and air bubbles. The size distribution of particles reflects the number fraction (expressed in percent) of the particle population in different size categories.

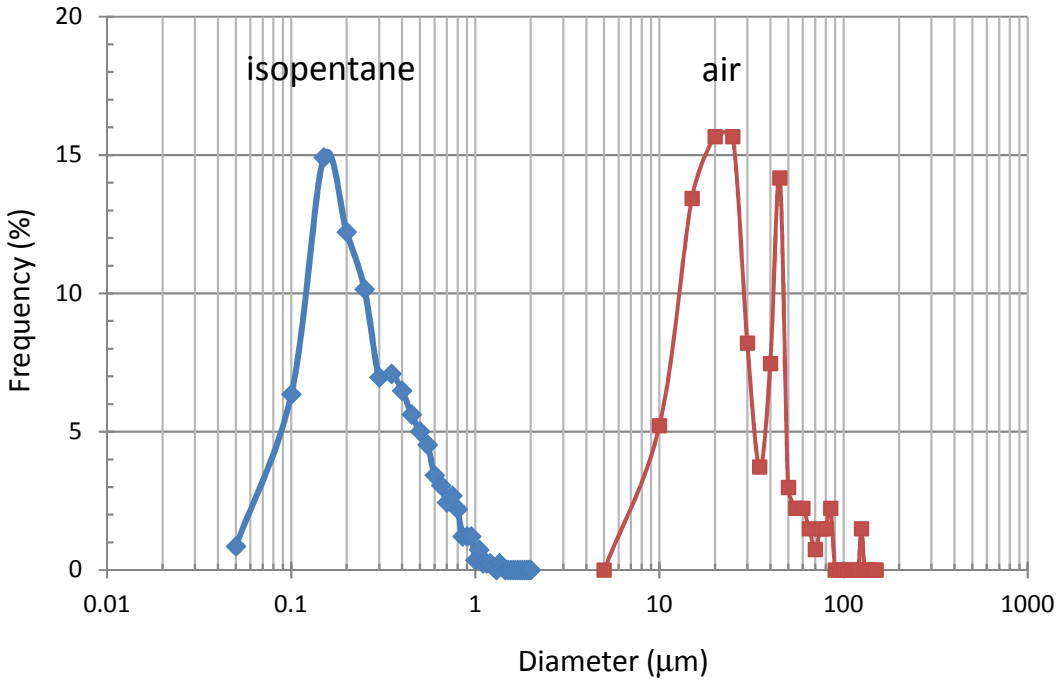


**Fig. 3.** Comparison of size distribution of air bubbles in premix A1 (> 130 measurements per data set) and isopentane droplets in premix A2 (> 800 measurements per data set).

Clearly, the size distributions of the two species do not overlap. The average diameter of isopentane droplets is around 360 nm and more than 37% of these pores are in the 100-250 nm range. In addition, none of the isopentane droplet is greater than 1.5 µm. By contrast, the size distribution of air bubbles is typically in the 5-125 µm range with an average value of 32 µm, which is two orders of magnitude larger than the average size of the isopentane droplets. At this point, it is worth mentioning that the samples (premix without PMDI) were not plunged into $LN_2$ immediately after the end of mixing. The delay, estimated to be around 20 min, may lead to a possible coarsening process. However, optical microscopy observations (not shown) reveal that this phenomenon predominantly applies to isopentane droplets. Because of Brownian motion, the micron-sized isopentane droplets dispersed in the polyol matrix are subjected to a multitude of collisions, which lead to an increase in their diameter by coalescence. On the contrary, coalescence of air bubbles may be slowed down or even prevented thanks to the presence of surfactant and because they are larger and relatively far from each other, while Ostwald ripening may still occur. As a result, the estimated initial size distributions (immediately after mixing) of isopentane droplets should be shifted towards smaller size (for $t$ = 0 s) thus increasing the gap between the size of isopentane droplets and air bubbles.

*3.2. Morphology of the AB systems before expansion ($t < t_{cream}$)*

In this part of this study, premix A2 was mixed with PMDI (cross-linking agent) leading to polyaddition reactions and foaming, simultaneously. Cryo-SEM micrographs exhibited in Figure 4 show the morphology of the AB1 system at 13 s ($t < t_{cream}$) after the addition of PMDI. This time period is well below the cream time ($t_{cream} \sim 20$ s) and thus ensures that the emulsion has not already expanded.

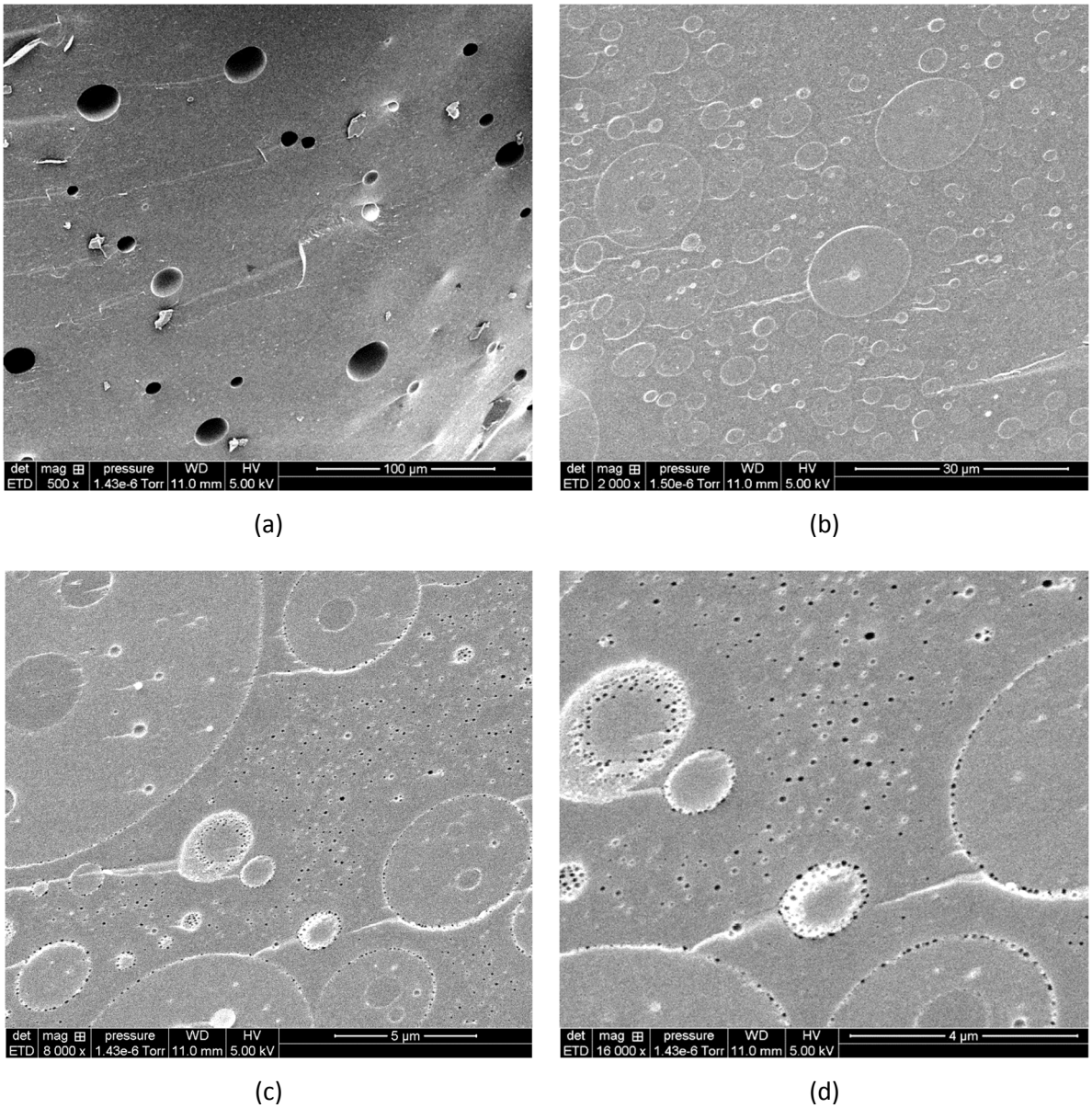


**Fig. 4.** Cryo-SEM micrographs of system AB1 (polyol/additives/isopentane mixed with PMDI) after 13 s and at different magnifications (a) x500, (b) x2000, (c) x8000 and (d) x16,000.

The low magnification view (x500) reported in Figure 4a shows the presence of the air bubbles ($d$ ~ 10.8 ± 5.7 µm) with a smooth and spherical shape. More importantly, the morphology depicted in Figure 4b at moderate magnification (x2000) reveals a typical dispersed phase/matrix morphology with the presence of dispersed nodules having an average diameter of about 2.4 ± 2.1 µm ($d_{min}$ ~ 0.45 and $d_{max}$ ~ 14.8 µm). It is clear from the above that polyol and PMDI are not molecularly mixed within the time scale investigated, even if partial miscibility is not excluded. The question which then needs to be answered is what phase is the matrix, polyol or PMDI? The answer to this question is not trivial because cryo-SEM images do not allow the identification of the different phases and because the morphology of emulsions depends on several parameters, such as formulation, composition, type of surfactant and viscosities of the phases.

The higher magnification view reported in Figure 4c reveals the presence of spherical sub-inclusions of the matrix material inside the dispersed phase nodules. This morphology is typical of multiple emulsions, sometimes called "double emulsions", which in fact are ternary systems ($_{PMDI}$/polyol/PMDI or $_{polyol}$/PMDI/polyol, the lower-case letter indicates the most internal phase) whereby the dispersed droplets contain smaller droplets of a different phase. There are also micro-size pores preferentially located inside the continuous phase which are very similar to those observed in Figure 2 (premix A2) and which can be attributed to isopentane droplets. As a reminder, isopentane was first introduced and dispersed into the polyol phase, but isopentane could migrate and/or diffuse inside the PMDI phase in order to reduce the interfacial free energy of the whole mixture. Surprisingly, the isopentane droplets are not distributed homogeneously inside the continuous phase, but a region of 0.5 to 1 µm in thickness surrounding each dispersed domain is free of isopentane droplet (free of micro-pore). Attempts have been made to prepare formulations without surfactant in order to determine whether the surfactant might be responsible of this kind of shield effect. Unfortunately, the formulation without surfactant was not stable enough and all the pentane quickly escaped from the mixture before the morphology was frozen-in.

Another important feature of Figure 4d is the presence of small cavities located at the polyol/PMDI interface. A first explanation is that they are due to isopentane droplets because they are similar in size. Other possible explanations can nevertheless be considered:

(i) It is generally admitted that water (premixed with the polyol) predominantly reacts with isocyanate to give carbon dioxide at the initial stage of foam rise. It is thus obvious to wonder whether the micro-cavities present at the interface between polyol and PMDI could be bubbles of carbon dioxide generated at the polyol/PMDI interface from the water-isocyanate reaction[13]. If true, these carbon dioxide bubbles should increase in size during foaming, either because more $CO_2$ will be produced or

because pentane molecules will diffuse inside these $CO_2$ bubbles. It will be shown in the next section that the opposite behavior is observed, which will refute that hypothesis.

(ii) Another possible explanation relates to a possible artifact of the cryo-SEM technique produced by the freezing of the mixture [8]. Indeed, if the coefficient of thermal expansion of polyol and PMDI are not the same, micro-void formation may occur at the interface during rapid cooling in $LN_2$. But why should these micro-voids take the same shape and size as isopentane droplets dispersed in the continuous phase rather than a simple void? It is certainly not fortuitous and, in an attempt to find out which explanation is the most plausible, the morphology of the AB2 system (i.e. without isopentane) was investigated. The cryo-SEM micrograph after 14 s ($t < t_{cream}$) of system AB2 is reported in Figure 5b and compared to the AB1 system at the same magnification (Figure 5a).

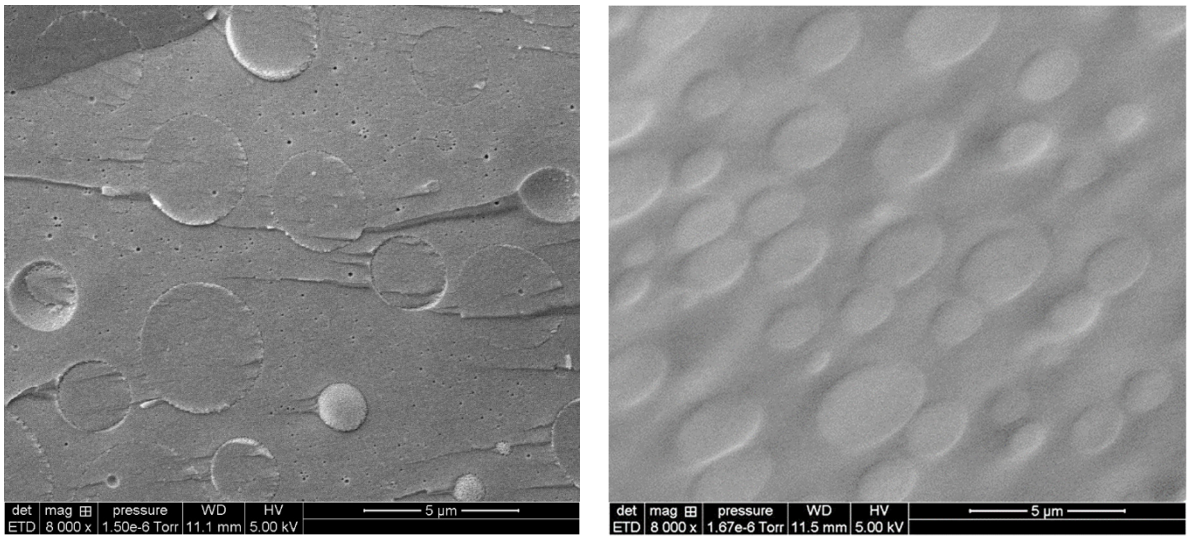


(a) (b)

**Fig. 5.** Cryo-SEM micrographs of (a) system AB1 containing isopentane (polyol/additives/isopentane mixed with PMDI) after 13 s, (b) system AB2 without isopentane (polyol/additives mixed with PMDI) after 14 s; Magnification x8000; scale bars 5 µm.

Figure 5b indicates that both the matrix and the interface between the polyol and PMDI appear smooth (without any void) in the AB2 system (without isopentane). It can thus be concluded that (i) the coefficients of thermal expansion of polyol and PMDI are rather similar; and (ii) that the micro-size pores located at the interface between the matrix and the dispersed phase come from isopentane droplets (and not from $CO_2$ generated by the water-NCO reaction). The presence of micro-droplets of isopentane stabilized by the surfactant and located at the PMDI/polyol interface may be explained by a phenomenon similar to the well-known “Pickering effect”. The stabilized isopentane droplets behave

like nano-objects localizing at the interface, thus lowering the interfacial energy of the PMDI/polyol interface. Finally, the size of the dispersed phase nodules is slightly smaller and the size distribution is narrower when isopentane is removed from the AB system (nodule diameter: $d \sim 2.37 \pm 2.11$ µm *vs* $d \sim 1.79 \pm 0.54$ µm for AB1 and AB2, respectively), which suggests a more stable emulsion (larger interfacial area).

A major question remains open: which phase (polyol or PMDI) is the continuous phase? Since isopentane was initially added to the polyol phase before addition of the PMDI, it would be tempting to conclude from Figure 4 ($t \sim 13$ s) that the continuous phase is the polyol-rich phase because isopentane droplets are seen there. To verify that hypothesis, isopentane was added to the PMDI phase (system AB3) instead of adding it to the polyol phase. The corresponding cryo-SEM micrographs taken at a time of 11 s after the start of mixing and exhibited in Figure 6 indicate that the morphology is not very different from that shown in Figure 4.

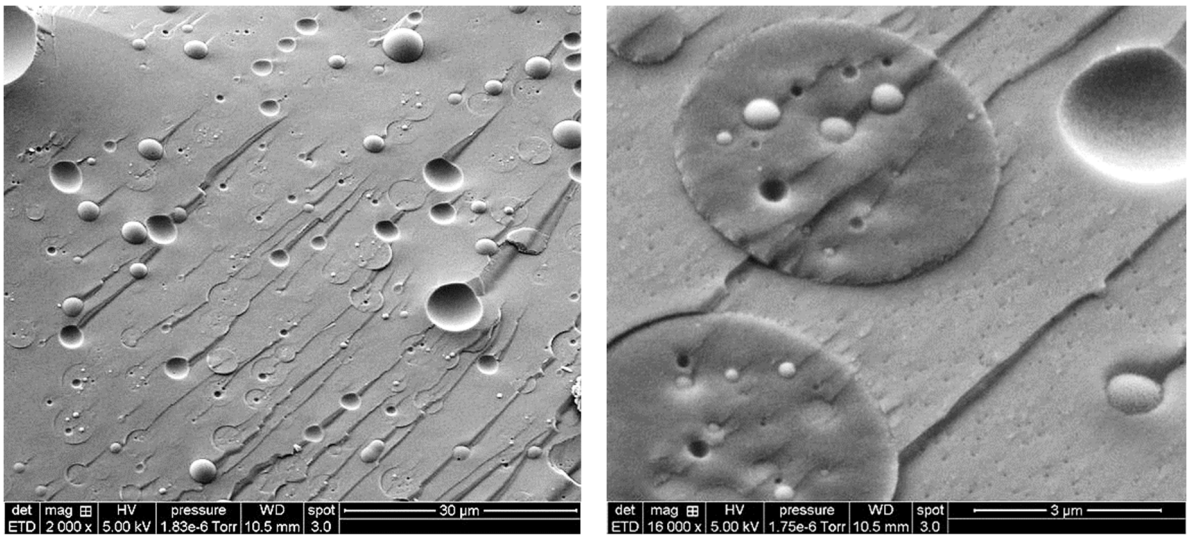


(a) (b)

**Fig. 6.** Cryo-SEM micrographs of system AB3 (polyol/additives mixed with PDMI/isopentane) after 11 s and at different magnifications (a) x2000, and (b) x16000. Please note that isopentane was added to the PMDI phase instead of adding it to the polyol phase.

A typical dispersed phase/matrix morphology was found again with small cavities dispersed into the continuous phase and a depletion zone surrounding the dispersed nodules, although less visible than in system AB1 (Figure 4d). However, the small cavities which correspond to the isopentane droplets appear smaller than in Figure 4 (AB1 system). In addition, the lower magnification view of AB3 system

(Figure 6a) reveals a number of intact nodules, whereas all the nodules depicted in Figure 4b were broken down at the level of the fractured surface. This delamination is also clearly visible at the level of the sub-inclusions located in the dispersed nodules. The reason for this lack of adhesion has not been fully explored but it is the author's belief that this behavior reflects the delay of the curing reaction between the OH group of the polyol and the isocyanate groups of PMDI as reflected by the slower kinetics (both $t_{cream}$ and $t_{string}$ increase by about 50% when isopentane is premixed with PMDI). Attempts have been made to detect the presence of silicon atoms of the surfactant as well as the phosphorus and chlorine atoms of the flame retardant (TCPP) by Energy Dispersive X-Ray spectroscopy but the results were disappointing.

### *3.3. Evolution of the morphology of AB system during foaming ($t > t_{cream}$)*

After establishing an outlook on PUR foam morphology before expansion ($t < t_{cream}$), one of the most interesting questions is how the morphology of the PU matrix will develop during the course of network buildup and foam expansion. Bubbles were found to increase in size, as a result of diffusion of carbon dioxide and isopentane molecules from the matrix into the bubbles. In consequence, the partly foamed sample gets more and more fragile because of foam expansion, preventing the observation of large fracture surface areas in the final material (as a rule of thumb, a 30 kg/m$^3$ density foam only contains 3 % by volume of material). It was nevertheless possible to follow the evolution of the polyol/PMDI morphology with time on very small-scale surfaces.

#### *3.3.1. Morphology of AB1 system at $t \sim 24$ s*

Figure 7 shows the morphology of the AB1 system at a foaming time of $t \sim 24$ s, i.e. just a few seconds after the cream time. Air bubbles shown in Figure 7a are still round in shape and isolated from each over because of the low expansion ratio. The most striking fact displayed in Figure 7b and c is the difficulty in discerning the dispersed phase nodules, although they are still present with a seemingly rather constant size distribution. Indeed, the vast majority of micro-size pores specifically located at the interface between the continuous phase and the dispersed phase nodules (like a string of pearls) have disappeared, thus decreasing the image contrast. This observation confirms our previous hypothesis according to which the micro-size pores located at the polyol/PMDI interface are not carbon dioxide bubbles (they should at least expand with time through the diffusion of isopentane molecules, just like pre-existing air bubbles) but rather isopentane droplets. Nevertheless, the disappearing of isopentane droplets is not generalized throughout the whole surface area and a few

spots still contain tiny isopentane droplets, as shown in Figure 7d. Comparison of Figure 4d and Figure 7d (same magnification) indicates that the size of the isopentane droplets decreases with time. Meanwhile, the start of the interfacial reaction (creation of an interphase?) may increase the adhesion between the dispersed phase nodules and the continuous phase, thus reducing detachment between the two phases.

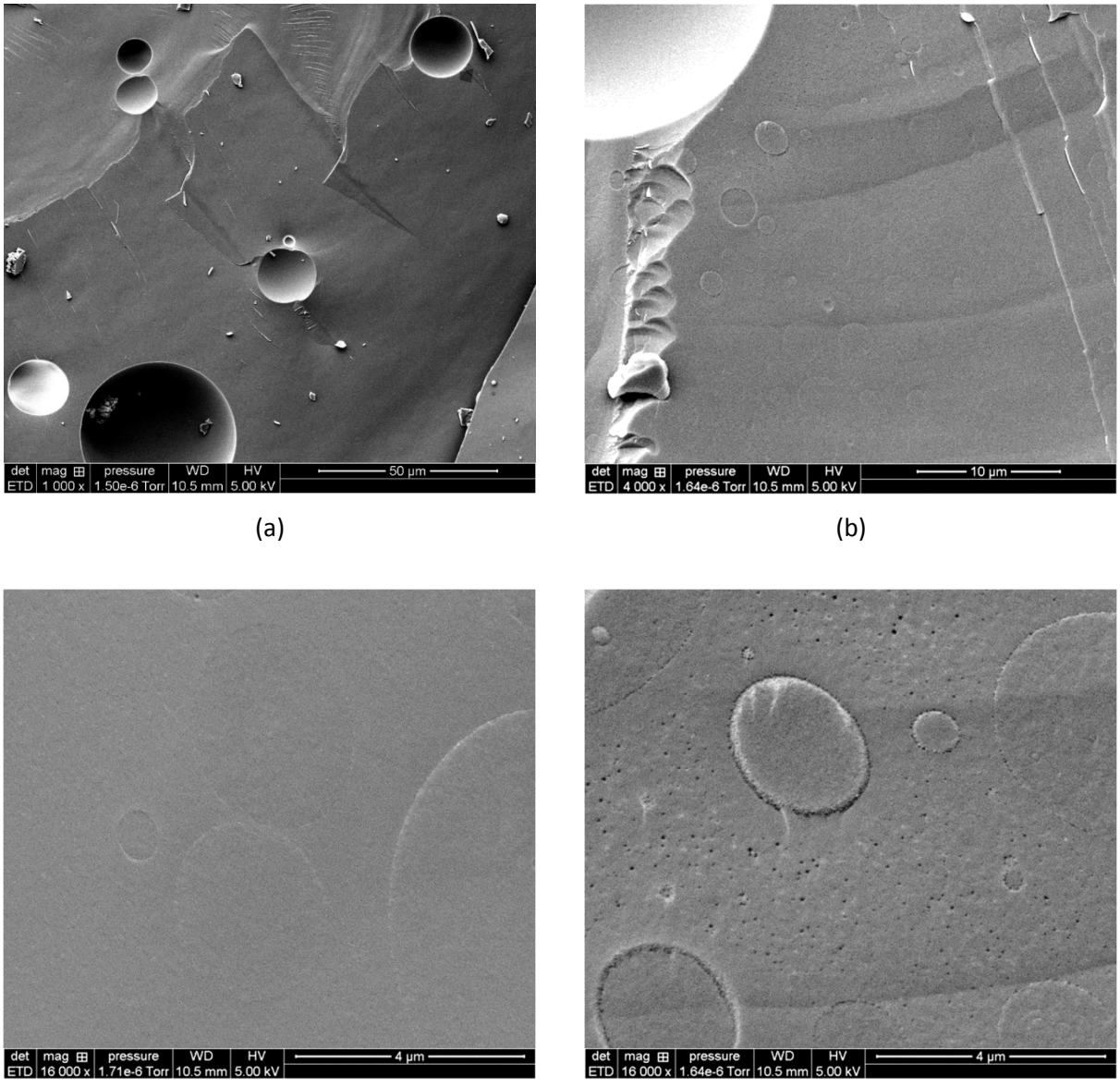


(a) (b)

(c) (d)

**Fig. 7.** Cryo-SEM micrographs of system AB1 (polyol/additives/isopentane mixed with PDMI) after 24 s and at different magnifications (a) x1000, scale bar 50 µm; (b) x4000, scale bar 10 µm; and (c) and (d) x16,000, scale bar 4 µm.

*3.3.2. Morphology of AB1 system at t ~ 37 s*

Figure 8a shows the morphology of the AB1 system at a foaming time of $t \sim 37$ s ($t_{cream} < t < t_{string}$) using the same settings on the cryo-SEM as those applied for the previous images. In a general manner, micro-size pores due to isopentane droplets have now completely disappeared and dispersed phase nodules are no more visible. But does it necessarily mean that the polyurethane material became homogeneous? In fact, we discovered by chance that the fracture surface of the dispersed phase nodules can be revealed by increasing the number of electrons received per surface unit and per time unit. This was accomplished by increasing the spot size and slowing down the scanning speed of the cryo-SEM. Figure 8 illustrates the evolution of the surface when several successive images of the same scanning area are taken with a higher spot size. As one progresses from Figure 8a to Figure 8d, it can be seen that the dispersed phase nodules are getting more and more visible, through the progressive appearance of well-defined wrinkles on their surfaces. Polyol and PMDI react differently to the electron beam, which results in a topological contrast between the phases.

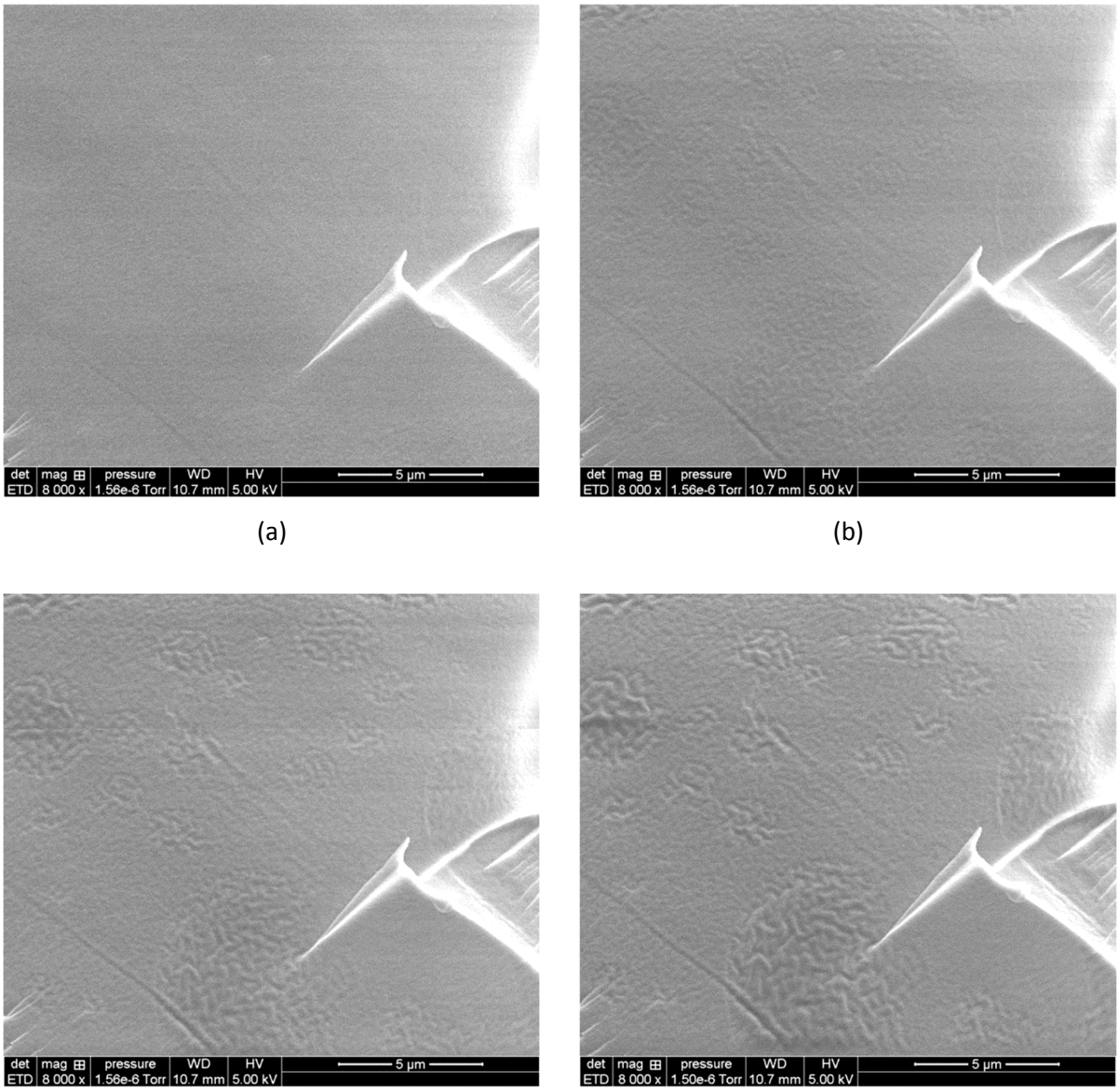


**Fig. 8.** Cryo-SEM micrographs of system AB1 (polyol/additives/isopentane mixed with PDMI) after 37 s with increasing spot size and slowing down the scanning speed (from a to d); Magnification of x8000, scale bar 5 µm.

The second important observation concerning the microstructure reported in Figure 8 is that the size of the dispersed phase nodules seems relatively constant with respect to shorter times, unlike isopentane droplets. An attempt has been made to estimate the surface fraction and the size of the dispersed phase nodules for the different foaming times investigated (*t*~13, 24 and 37 s). According to the values reported in Table 3 (at least 100 nodules were analyzed for each foaming time), no trend

appears in the size evolution of dispersed phase nodules within a timeframe of 37 s from the start of mixing of parts A and B (all values are in a range of statistical data spread).

**Table 3**. Comparison of volume fraction ($\chi_{vol}$) and average diameter ($d$) of dispersed phase nodules as a function of time.

| *time* (s) | $\chi_{vol}$ (%) | $d$ (μm) |
|---|---|---|
| 13 | 36.1 | 3.4 |
| 24 | 27.0 | 2.5 |
| 37 | 31.5 | 3.6 |

*3.3.3. Morphology of AB1 system at t ~ 50 s*

As next stage, Figure 9 shows the morphology of the AB1 system at a foaming time of $t$~ 50 s ($t_{cream} < t < t_{string}$) after dozens of scans of the same surface area at higher spot size and lower scanning speed, to get the chance to observe the dispersed phase nodules if they still existed. They were found to be indistinguishable from the continuous phase, even if the sample becomes rough at a very small scale. This may suggest that the polyurethane reactions are now sufficiently advanced to give a homogeneous material (as far as the electron beam is able to probe it).

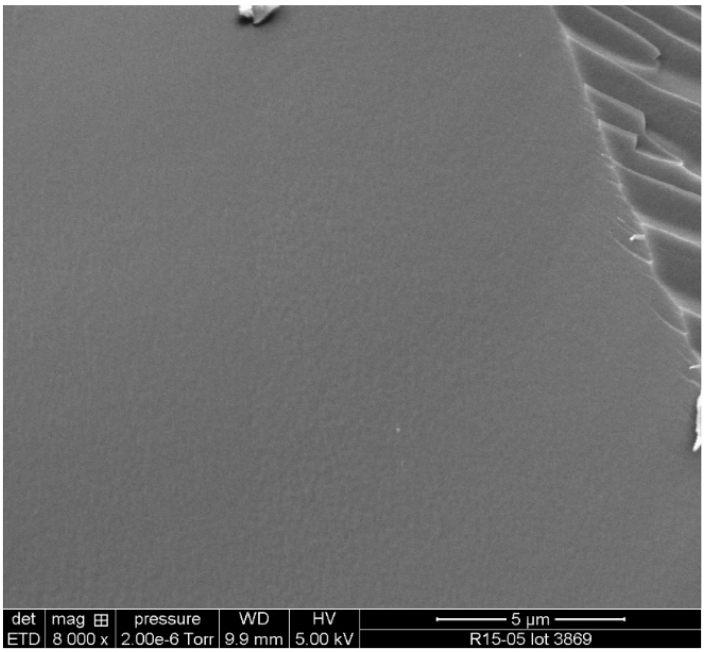


**Fig. 9.** Cryo-SEM image of system AB1 (polyol/additives/isopentane mixed with PDMI) after 50 s and at a magnification of x8000.

## 4. Discussion

### *4.1. Morphology of the AB mixture and its evolution during foaming*

The morphology of the AB1 system ($t < t_{cream}$) depicted in Figure 4 unambiguously indicates that the polyether polyol and the polymeric 4,4-diphenylmethane diisocyanate (PMDI) either are not miscible or do not have enough time to completely mix during the stirring stage time scale (5 s). Does it represent an isolated case? Until the end of the 1970s, three-component urethane polymerizations were treated as well mixed homogeneous reactive systems (i.e. at a molecular scale), resulting in the formation of random block copolymers. However, it has been shown that it is not always the case because of monomer incompatibility or imperfect mixing due to very short reaction times. For instance, Chen *et al.* investigated a model system based on 2,6 (or 2,4)-toluene diisocyanate (TDI) with 1,4-butanediol (BDO) as chain extender, and with hydroxy-terminated polybutadiene (PBD) as the soft segment and observed by optical microscopy BDO droplets (with diameter in the order of 5-50 µm) dispersed in a PBD-TDI continuous phase [14]. According to the authors, the final structure of the segmented PU was controlled by the reaction rates between the different functional groups and by the initial reactant incompatibility. Interestingly, most of the BDO droplets were still visible by optical microscopy and were found to maintain their shape and size at least up to 3 min after the addition of BDO while the system became stationary due to the increased viscosity. A number of studies were also

dedicated to the influence of impingement mixing on striation thickness (as defined by one half of the total width of two adjacent layers of alternate reactants) and properties of polyurethane elastomers in reaction injection moulding (RIM) process. When the mixing state was too coarse, Kolodziej et al. demonstrated that the reaction between MDI and polypropylene oxide (PPO) capped with ethylene oxide was controlled by the diffusion of the MDI molecules to the polyether polyol striation (the long prepolymer moved very slowly with respect to the small MDI molecules) [15]. On the contrary, the small chain extender molecules (BDO) were very mobile and could more easily diffuse from the polyol phase into the diisocyanate, leading to the formation of BDO-MDI hard segment layers. Lee et al. used a crosslinking polyester urethane system based on a poly-(ε-caprolactone) triol (PCL) and 4,4' diphenyl methane diisocyanate (MDI) with dibutyltin dilaurate (DBTDL) as catalyst and studied the effect of reaction rates (using different catalyst concentrations) and Reynolds number (*Re*) on the mixing quality [16]. They demonstrated that the polymerization was diffusion-controlled for high reaction rates as soon as the striation thickness was relatively large compared to molecular scale. In contrast, for slower reaction rates ($t_{gel}$ = 45-58 s), these authors explained that a much more complex model including both diffusion and chemical kinetics in a heterogeneous reaction system might be needed. In a different approach, Wickert et al. used a small RIM machine to produce 60 wt% hard segment polyurethane from pure MDI and a mixture of a polyether diol and BDO, which contained 0.005 wt% DBTDL [17]. Using light microscopy, these authors observed that the dispersed droplets swelled in size and explained that phenomenon by the diffusion of reactant molecules from the continuous phase to the dispersed phase.

A few interesting characteristics were also found in the scientific literature in the case of PU foam. Grünbauer et al. studied by Transmission Electron Microscopy (TEM) the morphology of $CO_2$-blown rigid polyurethane foam and observed irregularly spaced dark spots ($d$ ~ 50-300 nm), the number of which increased with increasing isocyanate index (defined by I=initial [NCO]/[active H]) and which were attributed to urea/urethane network precipitates [18]. By contrast, the presence of a few larger spots ($d$ ~ 1-1.5 μm), especially visible in the 0.3 and 0.4 isocyanate index was completely unexpected. According to the authors, these larger spots were reminiscent of the dispersion of isocyanate droplets in polyol at the early stage of mixing (before the polymerization), which does not mean that they had remained unaltered (in a chemical sense) during polymerization. Quite similar observations were reported by Priester et al. using TEM on MDI-based high resilience foam made at NCO indices of 0.8 and 1 and with various proportions of water (from 2.0 to 4.5 pphp) [19]. It was found that each of the samples contained discrete spherical phases ranging between 0.2 and 2.5 μm in diameter while the matrix appeared mottled (urea/urethane precipitates?). According to the authors, the discrete spherical phases were likely to be the result of an incompatible formulation and the most plausible

explanation was that they should correspond to MDI nodules. Despite the previous comments made by Grünbauer et al. [18] and Priester et al. [19], this does not necessarily mean that the dispersed nodules are also PMDI phase in our case. And the question remains whether PMDI is dispersed in polyol or polyol dispersed in PMDI. As a reminder, isopentane was added into the premix A2 followed by addition of PMDI with a syringe. It thus seemed logical from Figure 4 (AB1 system) to say that PMDI should be the dispersed phase and polyol the continuous phase since isopentane micro-droplets were located in the continuous phase. But everything was put into question when isopentane was first introduced into the PMDI phase (AB3 system, see Figure 6) because the morphology of the emulsion was very similar. To be frank, it is not even clear whether the nature of the continuous phase (polyol or PMDI) is the same in both cases because the kinetics reported in Table 2 are very different. But if this is the case, it would mean that isopentane droplets would have migrated very quickly from one phase to the other in one of the cases.

*4.2. Nucleation mechanism*

It is well recognized that the decrease in foam cell size is usually accompanied by the decrease in thermal conductivity following a mostly linear relationship [20-22]. In this context, a control of cell nucleation during foaming is a key factor for the control of the cellular morphology and consequently of the foam insulating efficiency. In the absence of experimental data, it was assumed in the past that foam formation began when the mixture became oversaturated with blowing agent molecules and that there was a possible phase separation (gas nuclei formation), according to the classical homogeneous nucleation theory [23]. This hypothesis was put into question by Kanner et al. who performed a direct visualization of foam expansion inside a pyrex glass cell and then suggested that self-nucleation was essentially absent in PU flexible foam blown with water as the only chemical blowing agent [12]. To verify that premise, they decided to saturate the polypropylene glycol/toluene diisocyanate solution (which was stable for several hours in the absence of catalyst) with the maximum possible $CO_2$ gas supersaturation level, i.e. as if all the $CO_2$ generated during the isocyanate-water reaction remained dissolved in the solution at the same time. No evidence of bubble formation was obtained when saturation pressure was released at both temperatures of 25 and 100°C, excepted the presence of insignificant trails of bubbles which appeared from several spots on the glass wall. The authors concluded that all bubbles which were growing in size during foaming were introduced by the process of mixing and that the number of bubbles at early times was more than sufficient to account for all of the cells present in the final foam. In other words, a direct relationship between the number of air bubbles present in the reaction mixture, the number of cells in the final foam product and their

average size should exist. As another proof, these authors obtained a foam with a coarse cellular structure when bubble introduction by mixing was deliberately held to a minimum. Baumhäkel studied the influence of stirring velocity and air loading on the formation of flexible urethane foams (water was used as the only chemical blowing agent) in an open container [24]. He demonstrated that the number of cells per $cm^3$ of foam linearly increased with agitator speed up to 3000 RPM. Nonetheless, Grünbauer et al. mentioned in a book chapter dedicated to rigid polyurethane foams that some doubts still subsisted whether nucleation could really occur by $CO_2$ formed (possibly at the polyol/PMDI interface) from the $H_2O$-PMDI reaction which is also known to occur during the early stage of the foam rise process [13]. As an example, Hager et al. dynamically monitored the interfacial mixing process of various systems by video microscopy techniques when two liquid boundaries were put into contact and reported the formation and growth of gas bubbles in the polyol phase when toluene diisocyanate (TDI) was contacted with polyol containing 4% water, with or without 0.2% bis (2-dimethylaminoethyl) ether as catalyst [25]. In our study, cryo-SEM images seem to demonstrate that nucleation of bubbles does not occur at the interface between polyol and PMDI. This comes back to the nowadays generally admitted idea that $CO_2$ molecules generated during the reaction of isocyanate with water cannot generate new bubbles during PUR foaming.

By contrast, a degree of confusion still prevails when physical blowing agents are added and in particular if the miscibility of the physical blowing agent is low. A typical example is given in the work of Volkert who prepared PUR foams with different perfluoro-alkanes ($C_5F_{12}$, $C_6F_{14}$ and $C_7F_{16}$ with boiling points of 29, 57 and 80°C, respectively) as blowing agents [26]. Perfluoro-alkanes were mainly insoluble in both the polyol and PMDI and thus resulted in an emulsion (droplet sizes were between 1 and 3 µm) when mixed with polyol and/or PMDI. Cellular materials with particularly fine cells ($d_{average}$~117 µm) and low thermal conductivity ($\lambda_{initial}$ ~ 18.1 mW/m.K) were obtained despite the molar ratio $CO_2$/perfluoro-alkanes of 89/11. It was claimed by the author that the heat released during reaction between the isocyanate (NCO) and the hydroxyl groups (OH) of water was sufficient to evaporate the droplets. In other words, it is asserted that vapor bubbles would have been created from the perfluoro-alkanes droplets instead of diffusing into the pre-existing air bubbles. This conclusion may seem surprising whereas a detailed view of a perfluoro-alkane/$CO_2$ foam obtained by laser fluorescence microscopy showed emulsified perfluoro-alkane micro-droplets inside the cell struts, thus indicating that perfluoro-alkane droplets have not yet vaporized. Other authors consider that the nucleation in PUR foaming is homogeneous and claim that liquid-type silane additives can act as efficient nucleating agents through the reduction of the surface tension, thereby decreasing the activation energy for nucleation (Gibbs free energy) and increasing the nucleation rate. For instance, the addition of 3 wt% of tetramethylsilane to a PUR foam formulation (cyclopentane/water 16.5/1.95) including a classical

surfactant (polysiloxane ether) was found to reduce the average cell size from 328 to 198 µm [27]. In the same way, hexamethyldisilazane was successfully used by Kang et al. to reduce the cell size of polyisocyanurate foams prepared with cyclopentane and water as blowing agents [28]. More generally, Grünbauer et al. underline that it is unclear whether nucleation in rigid foams should be characterized as homogeneous (new gaseous phase formation from nuclei) or as heterogeneous i.e. by formation of new gaseous phases at the interface of insoluble gas (such as $N_2$), liquid or solid perfluorinated particles (such as perfluoro-alkanes or polytetrafluoroethylene particles, respectively) [13]. But surprisingly, it is no longer a question of nucleation by air bubbles entrapped in the solution during mixing, while foam preparation usually implies the use of a mechanical stirrer in an open container which necessarily induces some air entrapment.

**Table 4**. Comparison between the different characteristics of air bubbles, isopentane droplets and cells (for details see the Appendix given in the Supplementary Material). *d* represents the average diameter of air bubbles, isopentane droplets or cells; $\chi_{i/A}$ represents the immiscible volume fraction of *i* component with respect to premix A; $\beta_i$ represents the population density of bubbles or droplets of *i* component.

| | *d* (µm) | $\chi_{i/A}$ (-) | $\beta_i$ (unity/cm$^3$) |
|---|---|---|---|
| Data for reference formulation AB1 before foaming | | | |
| Air bubbles | 32 | 0.11 | $3.06 \times 10^6$ |
| Isopentane droplets | 0.360 | 0.09 | $1.7 \times 10^{12}$ |
| Data for reference formulation AB1 after foaming (analysis of cellular structure in the plane perpendicular to the rise direction) | | | |
| PUR foam cells | 275 | NA | $2.3 \times 10^6$ |

Looking back on our particular case where the physical blowing agent (isopentane) is partially miscible with the polyol and/or PMDI, could the numerous isopentane droplets shown in Figure 4 ($t < t_{cream}$) vaporize and generate new bubbles (isopentane gas) when the temperature increases due to exothermic reaction between NCO and OH groups? This did not appear to be the case at first glance but to confirm this finding, cryo-SEM images were used to compare the number of isopentane droplets and the number of air bubbles present in the mixture (in the early times) with the cell population density of the final foam product (for details see the Appendix as given in the Supplementary Material). According to Table 4, the population density of air bubbles in the mixture (before expansion) compares well with the cell population density of the foam, which is typically in the order of $10^6$ cell/cm$^3$. On the

contrary, the isopentane droplet population density is about six orders higher than the cell population density of the final PUR foams. This result confirms our observations and demonstrates that isopentane droplets dispersed in the continuous phase cannot generate new bubbles during the course of foaming. Surprising at first, this phenomenon is closely related to the superheating (i.e. heating beyond the boiling point without actually boiling) of a dispersed droplet immersed in another nonvolatile liquid. In ordinary boiling, bubble formation usually occurs at a solid interface in contact with the liquid and is influenced by the presence of vapor/gas inclusions in impurities and/or on the wall of the structure containing the liquid. However, those nucleation sites can be eliminated if the volatile liquid is immersed in another nonvolatile liquid (intimate liquid/liquid contact) and in this case, the liquid must itself generate the vapor phase (i.e. must undergo a phase change). This implies the formation of a very small region of vapor (nucleus) in the volatile liquid which size should be higher than the critical radius, according to the classical homogeneous nucleation theory. As a result, the nucleation temperature of liquids was found to be much higher than the "normal" boiling point corresponding to the ambient pressure with a limit for pure liquids which can reach about 90% of the critical temperature (absolute temperature) at atmospheric pressure. For instance, it represents a difference of more than 100°C for isopentane ($T_L$~137°C) [29]. In addition, it was found that the presence of small gas bubbles (introduced by mechanical mixing or by a micro-syringe) inside the volatile droplet of butane or pentane can limit or even prevent superheating [30,31]. Interesting information are given in the review of Jones et al. on bubble nucleation from gas cavities [32]. According to these authors, bubble nucleation can be classified in 4 types. Types I and II nucleation correspond to the so-called classical homogeneous and heterogeneous nucleation theories, respectively. In both cases, the formation of a new gas phase necessitates to overcome a very high energy barrier in order to tear apart the liquid and counterbalance the high cohesive strength of the liquid. It requires high levels of supersaturation ($\sigma$) with values greater than 1000 ($\sigma$ is given by $\alpha$-1, where $\alpha$, the saturation ratio, is $C_2/C_{2s}$. $C_2$ and $C_{2s}$ are the concentrations of dissolved gas and the corresponding equilibrium concentration over a flat surface). On the contrary, types III and IV nucleation depend upon the existence of gas cavities and thus cannot be described by the classical theories. Indeed, the presence of gas cavities (or pre-existing bubbles) with radii of curvature greater than the critical value (as determined by the classical nucleation theory) has its nucleation energy barrier lowered to zero (type IV). In the case of type III, the radius of curvature of the pre-existing cavities is less than the critical radius at the moment the system is made supersaturated. Hence, there exists a finite nucleation energy barrier which must be overcome. The authors underlined that it is now widely accepted that most observed nucleation events originate from pre-existing cavities and are associated with low levels of supersaturation of 5 or less.

In our case, the presence of air bubbles dispersed in the matrix combined with the partial miscibility of isopentane into polyol and PMDI should favor the diffusion of isopentane molecules ($CO_2$ as well) toward these pre-existing air bubbles with no energy barrier to overcome (air bubbles are quite large with respect to the critical bubble radius, usually less than 1 µm). This phenomenon should limit the degree of superheating of isopentane droplets. To get more information on that, measurements of the temperature at the level of the sampling (i.e. a few millimeters under the top surface of the foam bun) during foaming are reported in Table 5 for the AB1 system and for the different morphologies described in the previous sections. As a reminder, isopentane droplets have almost completely disappear at t ~ 24 s which corresponds to a temperature of about 31.5°C, just a few Celsius degree above the boiling point of isopentane ($t_{boiling}$ = 27.8°C). In this context, it is thus not abnormal that the isopentane droplets do not create new bubbles, as suggested by the data reported in Table 4. Thus, isopentane droplets play the role of blowing agent reservoirs which empty as soon as isopentane molecules diffuse through the matrix into the pre-existing bubbles.

**Table 5**. Evolution of sample temperature (near the top surface of the bun) for AB1 system and for the different foaming times investigated.

| *time (s)* | *temperature (°C)* |
|---|---|
| 13 | 27.5±0.5 |
| 24 | 31.5±1.5 |
| 37 | 37.5±1.5 |
| 50 | 45±2 |

## 5. Conclusions

In the present work we have successfully visualized by cryo-SEM method the complex morphology of a growing realistic polyether-based PU matrix and its evolution with time during the very first moments of the foaming process. It is clearly demonstrated that the initial mixture possesses a heterogeneous structure composed, from the smallest to the largest, of sub-micron size isopentane droplets, micron size dispersed phase nodules and large air bubbles dispersed into a continuous matrix. However, there

is still some doubt as to whether polyol or PMDI is the continuous phase in this particular foaming system.

Following the evolution of the morphology of the AB system during foaming was made possible by the use of cryo-SEM and allowed suggesting an innovative vision of its initial stages: clearly, bubble nucleation ($CO_2$) formed from the $H_2O$-PMDI reaction did not occur at the interface between polyol and PMDI, as it has been sometimes suggested in the literature for high water content systems [13]. More importantly, it was indeed proven in our study that isopentane droplets (the undissolved part of the physical blowing agent) did not vaporize to create their own bubbles following homogenous nucleation of a vapor cavity in pure liquid (isopentane droplet) or the nucleation of a vapor cavity at the interface between two liquids (isopentane/continuous phase interface). Rather, these isopentane droplets were found to completely dissolve into the continuous phase with time before the majority of the heat release during reaction between the isocyanate and the hydroxyl groups of polyol and/or water did occur. The fact that this phenomenon appeared simultaneously with the growth of bubbles suggests that isopentane molecules constituting the droplets simply diffuse through the continuous phase into the preexisting air bubbles with time. As proof, the number of air bubbles per unit volume (~$10^6$ bubble/$cm^3$) was found to be in the same order as the cell population density of the final foam product (~$10^6$ cell/$cm^3$), while the number of isopentane droplets initially present per unit volume was found to be six orders of magnitude higher (~$10^{12}$ droplet/$cm^3$). These results also mean that the isopentane molecules dissolved in the matrix (certainly at low oversaturated level) cannot generate new bubbles on their own via formation of stable nuclei following the classical homogeneous nucleation theory, as it is too often claimed in the scientific literature for PUR foam prepared by mixing in an open-air container [4]. In consequence, it is not appropriate to calculate the Gibbs free energy of the homogeneous nucleation, except eventually if we would like to calculate the critical air bubble size that would be needed to have no energy barrier. In our case, this kind of nucleation is then considered as non-classical because there is no nucleation energy barrier to overcome (the radius of curvature of the initial air bubbles is greater than the critical nucleation value) and this corresponds to the type IV non-classical nucleation mechanism, as described by Jones et al. [32]. In other words, the phenomenon of air entrapment during the mixing stages appeared as the key element of the development of the cellular morphology which suggest that all parameters that can affect the number and size of air bubbles present in the initial mixing (viscosity of the phases including the influence of fillers, mixing device, speed of mixing, air pressure…) may potentially impact the final morphology of the PUR foam.

Several unexpected phenomena were encountered such as the presence of a depletion zone (free of isopentane droplets) around the dispersed phase nodules, associated with the localization of isopentane droplets at the interface between the continuous phase and the dispersed phase nodules.

Moreover, the respective locations of isocyanate and polyol could not be confirmed with absolute certainty. An artificial increase in the polyol phase volume through the addition of end-capped, nonreactive but otherwise similar polyol molecules could be a way of identifying those phases without a doubt while keeping the isocyanate index constant. Therefore, more work is needed to clarify these points with the ultimate goal to link the morphology of the starting emulsion with the cellular structure of the final foam product.

**Acknowledgements**

The "Centre Technologique des Microstructures, plateforme de l'Université Claude Bernard Lyon 1", CTμ is acknowledged for granting access to their equipment. The authors would like to thank Vincent Barraud, Jean-Pierre Pascault, Rémi Perrin and Alexandru Sarbu for helpful discussions. The authors would like to thank SOPREMA for financially supporting this research project.

**References**

[1] S. Pardo-Alonso, E. Solorzano, L. Brabant., P. Vanderniepen, M. Dierick, L. Van Hoorebeke, M.A. Rodríguez-Pérez, 3D analysis of the progressive modification of the cellular architecture in polyurethane nanocomposites foams via X-ray microtomography, Eur. Polym. J. 49 (2013) 999-1006

[2] M. Dabo, T. Roland, G. Dalongeville, C. Gauthier, P. Kékicheff, Ad-hoc modeling of closed-cell foam microstructures for structure-properties relationships, Eur. J. Mech A. Solids 75 (2019) 128-141

[3] E. Minogue, An in-situ study of the nucleation process of polyurethane rigid foam formation" Ph.D Thesis, Department of Chemical Sciences, Dublin City University, 2000

[4] S. Pardo-Alonso, E. Solorzano, S. Estravis, M.A. Rodriguez-Perez, J.A. de Saja, In situ evidence of the nanoparticle nucleating effect in polyurethane-nanoclay foamed systems, Soft Matter 8 (2012) 11262-11270

[5] Y. Zhao, M.B. Brown, S.A. Jones, Engineering novel topical foams using hydrofluoroalkane emulsions stabilised with pluronic surfactants, Eur. J. Pharm. Sci. 37 (2009) 370-377

[6] E.M. Ivan'kova, I.P. Dobrovolskaya, P.V. Popryadukhin, A. Kryukov, V.E. Yudin, P. Morganti, In-situ cryo-SEM investigation of porous structure formation of chitosan sponges, Polym. Test. 52 (2016) 41-45

[7] K.B. Caldwell, H.D. Goff, D.W. Stanley, A low-temperature scanning electron microscopy study of ice cream. I. Techniques and general microstructure, Food Structure 11 (1992) 1-9

[8] M.S. Zbik, J. Du, R.A. Pushkarova, R.St.C. Smart, Observation of gaseous films at solid-liquid interfaces: Removal by ultrasonic action, J. Colloid Interface Sci. 336 (2009) 616-623

[9] R.J. Mikula, V.A. Munoz, Characterization of emulsions and suspensions in the petroleum industry using cryo-SEM and CLSM, Colloids Surf., A, 174 (2000) 23-36

[10] Y. Talmon, The study of nanostructured liquids by cryogenic-temperature electron microscopy – A status report, J. Mol. Liq. 210 (2015) 2–8.

[11] J.C. Russ, R.T. Dehoff, Practical rheology, second ed., Springer Science + Business Media, LLC, 2000.

[12] B. Kanner, T.G. Decker, Urethane foam formation – Role of the silicone surfactant, J. Cell. Plast. 5 (1969) 32–39.

[13] H.J.M. Grünbauer, J. Bicerano, P. Clavel, R.D. Daussin, H.A. de Vos, M.J. Elwell, H. Kawabata, H. Kramer, D.D. Latham, C.A. Martin, S.E. Moore, B.C. Obi, V. Parenti, A.K. Schrock, R. van den Bosch, Chapter 7: Rigid polyurethane foams in polymeric foams, mechanisms and materials, CRC Press LLC, 2004.

[14] C.H.Y. Chen, R.M. Briber, E.L. Thomas, M. Xu, W.J. MacKnight, Structure and morphology of segmented polyurethanes: 2. Influence of reactant incompatibility, Polymer 24 (1983) 1333–1340.

[15] P. Kolodziej, C.W. Macosko, W.E. Ranz, The influence of impingement mixing on striation thickness distribution and properties in fast polyurethane polymerization, Polym. Eng. Sci. 22 (1982) 388–392.

[16] L.J. Lee, J.M. Ottino, W.E. Ranz, C.W. Macosko, Impingement mixing in reaction injection molding, Polym. Eng. Sci. 20 (1980) 868-874

[17] P.D. Wickert, W.E. Ranz, C.W. Macosko, Small scale mixing phenomena during reaction injection moulding, Polymer 28 (1987) 1105-1110

[18] H.J.M. Grünbauer, J.C.W. Folmer,Polymer morphology of $CO_2$-blown rigid polyurethane foams: Its fractal nature, J. Appl. Polym. Sci. 54 (1994) 935-949

[19] R.D.Jr Priester, R.B. Turner, Chap.4: The morphology of flexible polyurethane matrix polymers in Low Density Cellular Plastics, Physical Basis and Behavior, Edited by N.C. Hilyard and A. Cunningham, Springer-Science+Business Media, 1994

[20] G.W. Ball, R. Hurd, M.G. Walker, The thermal conductivity of rigid urethane foams, J. Cell. Plast. 6 (1970) 66-75

[21] L.D. Booth, W.M. Lee, Effects of polymer structure on K-factor aging of rigid polyurethane foam, J. Cell. Plast. 21 (1985) 26-30

[22] H. Lim, S.H. Kim, B.K. Kim, Effects of silicon surfactant in rigid polyurethane foams, eXPRESS Polym. Lett. 2 (2008) 194-200

[23] P.M. Wilt, Nucleation rates and bubble stability in water-carbon dioxide solutions, J. Colloid Interface Sci. 112 (1986) 530-538

[24] R. Baumhäkel, Influence of stirring velocity and air loading on the formation of flexible urethane foams, J. Cell. Plast. 8 (1972) 304-310

[25] S.L. Hager, T.A. Craig, M.W. Jorgenson, L.D. Artavia, C.W. Macosko, Interfacial mixing of urethane foam chemicals, J. Cell. Plast. 30 (1994) 44-58

[26] O. Volkert, PUR foams prepared with emulsified perfluoroalkanes as blowing agents, J. Cell. Plast. 28 (1992) 486-495

[27] J.W. Kang, J.M. Kim, M.S. Kim, Y.H. Kim, W.N. Kim, W. Jang, D.S. Shin, Effects of nucleating agents on the morphological, mechanical and thermal insulating properties of rigid polyurethane foams, Macromol. Res. 17 (2009) 856-862

[28] M.J. Kang, Y.H. Kim, G.P. Park, M.S. Han, W.N. Kim, S.D. Park, Liquid nucleating additives for improving thermal insulating properties and mechanical strength of polyisocyanurate foams, J. Mater. Sci. 45 (2010) 5412-5419

[29] C.T. Avedisian, The homogeneous nucleation limits of liquids, J. Phys. Chem. Ref. Data 14 (1985) 695-729

[30] S. Sideman, Y. Taitel, Direct-contact heat transfer with change of phase: Evaporation of drops in an immiscible liquid medium, Int. J. Heat Mass Transfer, 7 (1964) 1273-1289

[31] Y. Tochitani, Y.H. Mori, K. Komotori, Vaporization of single liquid drops in an immiscible liquid, Part I: Forms and motions of vaporizing drops, Wärme- und Stoffübertragung, 10 (1977) 51-59

[32] S.F. Jones, G.M. Evans, K.P. Galvin, Bubble nucleation from gas cavities – A review, Adv. Colloid Interface Sci. 80 (1999) 27-50

**Appendix**

*A.1. Cell population density of the final foam product*

The cell population density of a foam product, as defined by the number of cells per unit volume of the original unfoamed polymer, was evaluated using the following equation

$$\beta \cong \frac{6\times10^{+12}\left[\left(\rho_p/\rho_f\right)-1\right]}{\pi d^3} \qquad \text{(A1)}$$

where $\beta$ is the cell population density (cell/cm$^3$), $d$ the average diameter of the cells (µm), $\rho_p$ and $\rho_f$ the densities of the unfoamed and foamed polymer respectively ($\rho_p$~*1200 kg/m$^3$* and $\rho_f^{réelle}$ ~*31.1 kg/m$^3$*). To take into account the shape factor of the cells (R ~ 1.5), $\rho_f$ was multiplied by a factor 1.5 which corresponds to the reduction of foam volume to get a shape factor equal to unity ($\rho_f^{corrected}$ ~ *46.7 kg/m$^3$*). The average cell diameter was multiplied by 1.2739 (according to ASTM D 3576-98) to take into account the relationship between the diameter obtained from the surface area of the cells (2D SEM images) and the real diameter of the cells ($d_{corrected}$ ~ 275 µm). Eventually, the cell population density was estimated to $\beta_{cell}$ ~ 2.3x10$^6$ cell/cm$^3$ which is typical of $\beta$ values reported in the scientific literature for PUR foams prepared by the hand mix technique.

*A.2. Cell population density of air bubbles and isopentane droplets in the AB system before expansion*

The number of air bubbles and isopentane droplets is more difficult to estimate since this cannot be done on the PU rigid foam product. In a general way, the population density of bubbles or droplets of *i* component is given by

$$\beta_i = \frac{number\ of\ bubbles\ or\ droplet\ of\ i\ component}{V_{total}} \qquad \text{(A2)}$$

where $V_{total}$ represents the total volume of AB system before expansion, including air bubbles entrapped during mixing. In first approximation, we will consider here that the size and number of i component (air bubbles and isopentane droplets) inside the AB system is the same as in the premix A. It can thus be written that

$$number\ of\ bubbles\ or\ droplets\ of\ i\ component = \frac{\chi_{i/A}.V_A}{V_i} \qquad \text{(A3)}$$

where $\chi_{i/A}$ represents the immiscible volume fraction (the miscible part is not taken into account in the calculation) of *i* component with respect to premix A, $V_i$ the average volume of one air bubble or one

isopentane droplet of component i, $V_A$ the total volume of premix A. On the other hand, the total volume of the AB system (before expansion) can be estimated by

$$V_{total} = V_A + V_B = \frac{M_A}{\rho_A^{app}} + \frac{M_B}{\rho_B} \qquad \text{(A4)}$$

where $M_A$ and $M_B$ are the weight of A and B respectively, $\rho_A^{app}$ and $\rho_B$ the apparent density of premix A and phase B ($\rho_B$ = 1230 kg/m$^3$ according to the supplier), respectively. The number of bubble or droplet of component *i* is given by the relation

$$\beta_i = \frac{\chi_{i/A} V_A}{V_i} / V_{total} \qquad \text{(A5)}$$

By replacing $V_i$ by the volume of a sphere of $d_i$ diameter, and a few simplifications, one obtains the following equation

$$\beta_i = \frac{6\chi_{i/A} M_A \rho_B}{\pi d_i^3 \left(M_A \rho_B + M_B \rho_A^{app}\right)} \qquad \text{(A6)}$$

Estimating the volume fractions of air bubbles and isopentane droplets inside the premix A ($\chi_{i/A}$) is likely to be the trickiest part of the exercise. For that purpose, 100 cm$^3$ of premix A (including air bubbles entrapped during the mixing stages) were put into a 100 cm$^3$ cylindrical test tube and sealed. First, the apparent density of the premix was estimated from the net mass and volume of premix A which gives $\rho_A^{app}$ ~ 0.944 g/cm$^3$ (for comparison purpose, the density of pure polyol is $\rho_{polyol}$ = 1,13 g/cm$^3$ according to the supplier). Then the premix was kept at rest during a few days. Upon creaming, it separates into two different phases: the upper phase is transparent and colorless and should mainly contain isopentane. The bottom phase is viscous and yellow and should mainly contain polyol. It is worth noting that polyol may still contain isopentane molecules which are dispersed at a molecular scale and which are small enough and stabilized by the surfactant to avoid buoyancy. In other words, it is assumed that the volume of the isopentane-rich phase corresponds to the volume of pentane which is mainly present as isopentane droplets inside the premix A. Obviously, the total volume of premix was found to decrease during creaming when air bubbles were progressively released at the surface of the liquid because the density of air bubbles ($\rho_{air}$ ~ 0,0012 g/cm$^3$) is 3 orders of magnitude lower than that of the polyol. The volume of the different liquid phases was measured which gives $\chi_{isopentane/A}$ ~ 0.09, $\chi_{polyol/A}$ ~ 0.8 and $\chi_{air/A}$ ~ 0.11. By using $M_A$ = 119.6 g, $M_B$ = 170.74 g, $\rho_{MDI}$ = 1.23 g/cm$^3$ , the population densities of air bubbles and isopentane droplets in the AB system can thus be estimated from equation A6 which gives $\beta_{air}$ ~ 3.06x10$^6$ bubble/cm$^3$ and $\beta_{isopentane}$ ~ 1.7x10$^{12}$ droplet/cm$^3$.